

Near-Field Wideband Beamforming for Extremely Large Antenna Arrays

Mingyao Cui, Linglong Dai, Robert Schober, and Lajos Hanzo

Abstract

The deployment of wideband extremely large antenna arrays has the promising of achieving Tbps data rates in the next-generation communication networks. However, due to the extremely wide bandwidth and large antenna array aperture, the near-field beam-split effect will severely degrade the actual transmission rates, which has not been investigated in existing works. To address this challenging problem, we first reveal the near-field beam-split effect and analyze the corresponding array gain loss. Then, a piecewise-far-field model with piecewise-linear phase characteristics is harnessed for approximating the near-field channel. Based on this, we conceive a phase-delay focusing method for mitigating the near-field beam-split effect. Moreover, we introduce a new metric, termed the effective Rayleigh distance, which is more accurate in distinguishing the far-field and near-field regions than the classical Rayleigh distance for practical communications. Finally, numerical results are provided to demonstrate the effectiveness of our methods.

Index Terms

Extremely large antenna array, wideband, near-field beam-split, beamforming, Rayleigh distance.

M. Cui and L. Dai are with the Beijing National Research Center for Information Science and Technology (BNRist) as well as the Department of Electronic Engineering, Tsinghua University, Beijing 100084, China (e-mails: cmy20@mails.tsinghua.edu.cn, daill@tsinghua.edu.cn).

R. Schober is with the Institute for Digital Communications at Friedrich-Alexander University Erlangen-Nürnberg (FAU) (e-mail: robert.schober@fau.de).

L. Hanzo is with the Department of Electronics and Computer Science, University of Southampton, Southampton SO17 1BJ, U.K. (e-mail: lh@ecs.soton.ac.uk).

This work was funded in part by National Key R&D Program of China (No.2020YFB1805005) and in part by the National Natural Science Foundation of China (Grant No. 62031019).

I. INTRODUCTION

Large antenna arrays improve the transmission rate by orders of magnitude, hence they had become a key technology in current communication systems [1]. Indeed, they are evolving to extremely large antenna arrays [2], where the array aperture is dramatically increased for supporting ultra-high speed transmission in various scenarios, e.g., 6G networks [3]–[5], Wi-Fi systems [6], and visible light communications [7]. In 6G communications, extremely large arrays may be utilized for distributed multiple-input-multiple-output (MIMO) systems relying on *radio stripes* [3] and for reconfigurable intelligent surface (*RIS*) [4], [5] to provide ultra-high beamforming gains to improve spectrum efficiency. Furthermore, it has been proposed to deploy extremely large arrays coating on entire walls to enhance coverage of Wi-Fi7 (IEEE 802.11be), [6], [8]. Moreover, extremely large arrays also offer opportunities for satellite, unmanned aerial vehicle (UAV), and offshore communications [9], [10]. On the other hand, benefiting from the enormous spectrum resources available in the millimeter wave and terahertz bands, high-frequency communications can provide a very wide bandwidth (e.g., several GHz) [11]. The very small size of high-frequency antennas also favorably enables the deployment of extremely large arrays [12]. Therefore, wideband extremely large arrays are promising for next-generation wireless networks [13].

A. Prior Works

The evolution from large arrays to extremely large arrays not only implies an increase in array aperture, but also leads to a fundamental change of the characteristics of the electromagnetic field. The electromagnetic radiation field can be divided into the far-field and near-field regions [14], [15]. In the far-field region, the channel can be modeled under the **planar wave** assumption, where the phase of the array response vector is a *linear* function of the antenna index [16]. In contrast, the near-field channel has to be modeled under the **spherical wave** assumption, where the phase of the array response vector is a *non-linear* function of the antenna index [14]. The boundary between near field and far field is popularly quantified by the Rayleigh distance [17], which is proportional to the square of the array aperture and inversely proportional to the wavelength. Since the array aperture is typically not very large in the current systems, the near-field range is negligible. In this case, the classical beamforming techniques generate planar wavefront beams propagating in the desired directions. By contrast, as the number of antennas increases dramatically for extremely large arrays, the near-field range will be expanded by orders

of magnitude. Typically, the Rayleigh distance of extremely large arrays can be up to several hundreds of meters, which covers a large part of typical cells. In this case, near-field beamforming is carried out to focus the beams with spherical wavefront around the desired user location [18], which is decided by the direction and the distance between the base station and the user. Given this non-negligible near-field range, near-field communications will be of pivotal significance in next-generation communications.

Moreover, when it comes to wideband systems, large antenna arrays tend to rely on phased array-based beamforming architecture [19], which can only realize *frequency-independent* narrowband beamforming. Due to the extremely wide bandwidth, the generated beam wavefronts at different frequencies will deviate from that at the center frequency, which is termed as the beam-split effect [20]. Specifically, in the far field scenarios, the beam-split effect will result in beams propagating in different directions at different frequency components [21], which is similar to rainbows caused by the dispersion of white light [22]. In contrast, in the near field scenarios, the beam-split effect results in a new phenomenon that the beams at different frequencies are focused at different directions and different distances, and thus the signal energy fails to focus on the desired receiver location. Consequently, only the beams around the center frequency can be recovered by the receiver, while most of the beams over the entire bandwidth will suffer from a serious array gain loss.

Since the array aperture is not very large in the operational systems, existing works have focused on the far-field beam-split problem. The corresponding solutions can be generally classified into two categories, i.e., algorithmic methods and the hardware-based mitigation methods. For the first category of solutions, by carefully optimizing the phase shifts (PSs) of the phased array, wide beams are generated to alleviate the beam-split effect [20], [23]–[25]. However, since these methods either heavily depend on the planar wavefronts in the far-field region [20], [23], or assume the bandwidth to be not very large [24], [25], they are not applicable for near-field wideband systems. For the second category of solutions, a large time-delay (TD) array rather than a classical phased array is employed to generate *frequency-dependent* beams, which can nearly eliminate the beam-split effect [26], [27]. Unfortunately, large TD arrays introduce much higher power consumption than large phased arrays. Thus, it is impractical to deploy large TD arrays [27]. To the best of our knowledge, the near-field beam-split effect has not been studied in the literature and corresponding solutions are not applicable so far.

B. Our Contributions

In this paper, we propose a phase-delay focusing (PDF) method to address the near-field beam-split problem. Our key contributions can be summarized as follows.

- We first reveal the near-field beam-split effect for extremely large arrays, and then analyze the array loss it causes.
- Then, to overcome the array gain loss, we first propose a piecewise-far-field model to approximate the near-field model with high accuracy in a piecewise-linear manner, where the entire large array is partitioned into multiple small sub-arrays. In this way, the receiver is located in the far-field region of the small sub-arrays but in the near-field region of the entire large array. Inspired by this piecewise-far-field model, we insert a TD element between the PSs and the radio-frequency (RF) chain for each sub-array. Then, through joint control of the delay and the phase to match the piecewise-far-field channel model, a phase-delay focusing (PDF) method is proposed to focus the beams over the entire bandwidth on the desired user location. Therefore, the near-field beam-split effect is effectively mitigated.
- Furthermore, from the perspective of the array gain, a new metric, called effective Rayleigh distance, is introduced to distinguish far field and near field. Compared to the classical Rayleigh distance defined from the perspective of phase errors, since the array gain directly influence the transmission signal-to-noise ratio (SNR), the proposed effective Rayleigh distance is a more accurate metric to measure the near-field range for practical communications.
- Finally, simulation results are provided to validate the proposed PDF method, which can mitigate the near-field beam-split effect and realize a near-optimal rate performance.

II. NEAR-FIELD BEAM-SPLIT

In this section, we will reveal the near-field beam-split effect in wideband extremely large array systems. We suppose the base station (BS) is equipped with an N -element uniform linear array¹. The orthogonal frequency division multiplexing (OFDM) with M sub-carriers is employed. Variables $d = \frac{\lambda_c}{2}$, λ_c , c , $f_c = \frac{c}{\lambda_c}$, and B denote the antenna spacing, carrier wavelength, speed of light, center carrier, bandwidth, respectively. As shown in Fig. 1, suppose the midpoint of the BS array is located at $(0, 0)$ in the XY-plane, and then the coordinate of the n -th BS antenna

¹For simplicity, we consider a uniform linear array as an example in this paper. Note that the proposed scheme can be straightforwardly extended to other types of array, such as uniform planar arrays.

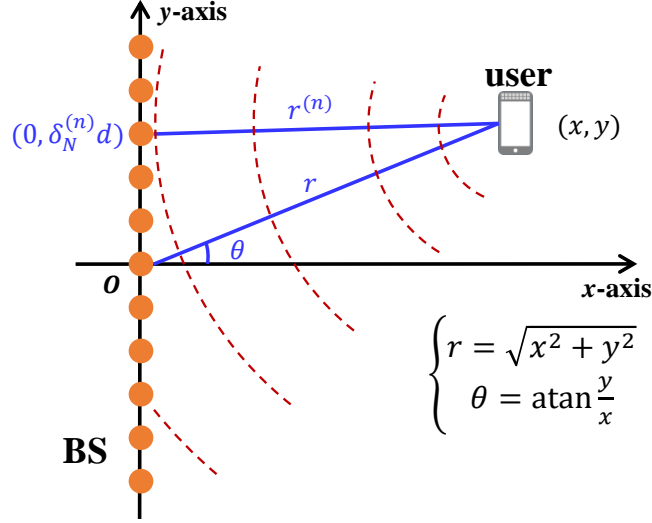


Fig. 1. The system layout of extremely large arrays.

is $(0, \delta_N^{(n)}d)$, where $\delta_N^{(n)} = n - \frac{N-1}{2}$ with $n = 0, 1, \dots, N-1$. Therefore, the array aperture is $D = N(d-1) \approx Nd$. A single-antenna receiver is located at (x, y) , where its polar coordinate is $(r, \theta) = (\sqrt{x^2 + y^2}, \arctan \frac{y}{x})$. Then, the line-of-sight near-field channel $\mathbf{h}(r, \theta, f_m) \in \mathbb{C}^{1 \times N}$ can be modeled under the spherical wave assumption [14] as

$$\mathbf{h}(r, \theta, f_m) = g_m \left[e^{-jk_m r^{(0)}}, e^{-jk_m r^{(1)}}, \dots, e^{-jk_m r^{(N-1)}} \right], \quad (1)$$

where $f_m = f_c + \frac{2m-M+1}{2M}B$ with $m = 0, 1, \dots, M-1$ denotes the m -th sub-carrier frequency, $k_m = \frac{2\pi f_m}{c}$ denotes the wavenumber at frequency f_m , and $|g_m| = \frac{c}{4\pi f_m r_n}$ denotes the free-space path loss [28]. $r^{(n)}$ denotes the distance between the n -th antenna and the user, satisfying

$$r^{(n)} = (x^2 + (y - \delta_N^{(n)}d)^2)^{\frac{1}{2}} = (r^2 + (\delta_N^{(n)}d)^2 - 2\delta_N^{(n)}dr \sin \theta)^{\frac{1}{2}} \quad (2)$$

For the traditional PS based beamforming, since it can only realize frequency-independent phase control [1], the near-field beamforming vector $\mathbf{w}(r, \theta) \in \mathbb{C}^{N \times 1}$ is usually determined based on the channel at the center frequency f_c [18], i.e.,

$$[\mathbf{w}(r, \theta)]_n = \frac{1}{\sqrt{N}} \arg([\mathbf{h}(r, \theta, f_c)]_n^*) = \frac{1}{\sqrt{N}} e^{jk_c r^{(n)}}, \quad (3)$$

where $[\mathbf{x}]_n$ denotes the n -th element of vector \mathbf{x} , $\arg(x)$ denotes the phase of x , and $k_c = \frac{2\pi f_c}{c}$ denotes the wavenumber at the center frequency f_c . Notice that the phase $k_m r^{(n)}$ in (1) or $k_c r^{(n)}$ in (3) is non-linear with respect to the antenna index n . Traditionally, since the array aperture is

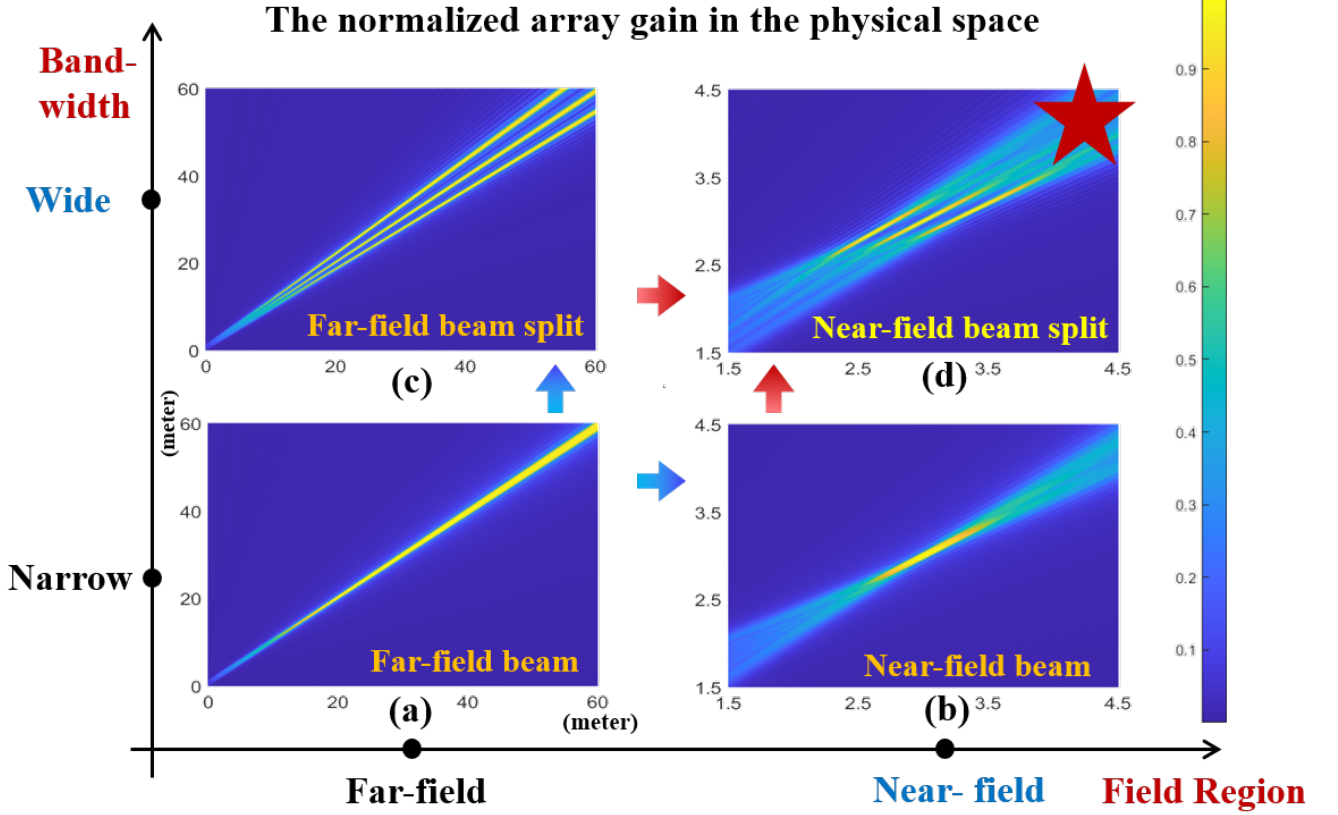


Fig. 2. This figure illustrates the normalized array gain in the physical space. We consider four scenarios: (a) the far-field narrowband scenario, (b) the near-field narrowband scenario, (c) the far-field wideband scenario, and (d) the near-field wideband scenario. In each sub-figure, the beam energy of the lowest, the center, and the highest frequencies are plotted (e.g., the three lines in the sub-figure (c) and (d)). Existing works mainly focus on the cases (a), (b), and (c), while case (d) has not been studied yet, and is the focus of this paper.

not very large, the far-field model under the planar wave assumption [16] is widely adopted to simplify the non-linear distance as

$$r^{(n)} = r \left(1 + \frac{(\delta_N^{(n)} d)^2}{r^2} - \frac{2\delta_N^{(n)} d \sin \theta}{r} \right)^{\frac{1}{2}} \stackrel{(a)}{\approx} r \left(1 - \frac{\delta_N^{(n)} d \sin \theta}{r} \right) = r - \delta_N^{(n)} d \sin \theta, \quad (4)$$

where (a) is derived by utilizing the first order Taylor expansion $(1+x)^{\frac{1}{2}} \approx 1 + \frac{1}{2}x$ and omitting the item $\frac{(\delta_N^{(n)} d)^2}{r^2}$. It is obvious from (4) that in the far-field, the phase becomes $k_m r^{(n)} \approx k_m r - k_m \delta_N^{(n)} d \sin \theta$, which is a linear function of the antenna index n . Then the far-field beamforming vector becomes $[\mathbf{w}(r, \theta)]_n = \frac{1}{\sqrt{N}} e^{jk_c r} e^{-jk_c \delta_N^{(n)} d \sin \theta}$. Since the item $e^{jk_c r}$ is a constant phase not relating to the antenna index n , $[\mathbf{w}(r, \theta)]_n$ can be rewritten as $[\mathbf{w}(r, \theta)]_n = \frac{1}{\sqrt{N}} e^{-jk_c \delta_N^{(n)} d \sin \theta} = [\mathbf{w}^{\text{far}}(\theta)]_n$, depending only on direction θ . In this case, as shown in Fig. 2 (a), the generated beam transmit signals towards the desired direction θ . However, since the linear phase approximation in (4) is not accurate when n is very large, the above far-field assumption does not hold anymore

for extremely large arrays. The typical near-field range is determined by the Rayleigh distance [28] $R = \frac{2D^2}{\lambda_c} = \frac{1}{2}N^2\lambda_c$. If the number of antennas N increases dramatically, the near-field region will expand by orders of magnitude. For instance, with 512 antennas and 100 GHz frequency, the Rayleigh distance is about 400 meters. In this case, the accurate spherical wave model has to be adopted for the channel $\mathbf{h}(r, \theta, f_m)$ in (1) and the beamforming vector $\mathbf{w}(r, \theta)$ in (3). Accordingly, as shown in Fig. 2 (b), the generated near-field beam focuses the signal energy around the desired location (r, θ) [29], which depends on both the distance and direction of the receiver. This procedure is also called beamfocusing [18] in the near-field.

The discussion above assumes that the bandwidth is not very large, as for wideband systems, a severe beam-split effect is induced. Specifically, employing the beamforming vector $\mathbf{w}(r, \theta)$, we define $G(\hat{r}, \hat{\theta}, r, \theta, f_m) = \left| \frac{1}{\sqrt{|g_m|^2 N}} \mathbf{h}(\hat{x}, \hat{y}, f_m) \mathbf{w}(r, \theta) \right|$ as the normalized array gain at frequency f_m on the location $(\hat{r}, \hat{\theta})$ with $\hat{r}^{(n)} = \sqrt{\hat{r}^2 + (\delta_N^{(n)} d)^2 - 2\delta_N^{(n)} d \hat{r} \hat{\theta}}$. Therefore, we have

$$G(\hat{r}, \hat{\theta}, r, \theta, f_m) = \frac{1}{N} \left| \sum_{n=0}^{N-1} e^{-j(k_m \hat{r}^{(n)} - k_c r^{(n)})} \right|. \quad (5)$$

Obviously, the maximum value of $G(\hat{r}, \hat{\theta}, r, \theta, f_m)$ is 1. In narrowband systems, $f_m \approx f_c$ holds, and the array gain $G(\hat{r}, \hat{\theta}, r, \theta, f_m)$ reaches its peak when $(\hat{r}, \hat{\theta}) = (r, \theta)$, which means that the beam energy is exactly focused at location (r, θ) . However, if $f_m \neq f_c$ in wideband systems, when $(\hat{r}, \hat{\theta}) = (r, \theta)$, since the phases $e^{-j(k_c - k_m)r^{(n)}}$ of different antennas n are different, the array gain $G(r, \theta, r, \theta, f_m)$ at frequency f_m will be significantly reduced. That is to say, the beam energy at f_m is split from the desired location (r, θ) . In the far-field, where the distance is large, as shown in Fig. 2 (c), this beam-split effect causes beams at different frequencies to split into different directions [30]. However, in the near-field, as shown in Fig. 2 (d), the beam-split effect causes beams at different frequencies to focus on different locations, and thus the receiver can only receive signals around the center frequency. For example, when we consider $f_c = 100$ GHz, $B = 5$ GHz, and $N = 512$, due to the near-field beam-split effect, more than 50% of the sub-carriers will suffer at least 60% array gain loss. Recent works mainly focus on mitigating the far-field beam-split effect. To this end, they either deploy a large number of high power consumption time-delay elements [26], [27], or heavily rely on the linear phase property of the far-field channel [20], [23]–[25], which is not valid in the near-field. To the best of our knowledge, the near-field beam-split effect has not been studied in the literature yet.

III. PROPOSED METHODS

In this section, first a piecewise-far-field channel with piecewise-linear phase is proposed to approximate the near-field channel, based on which we propose a PDF method to mitigate the near-field beam-split effect.

A. Piecewise-far-field Channel Model

Due to the non-linear phase $-k_m r^{(n)}$ against the antenna index n as shown in (1), it is intractable to directly design near-field wideband beamforming techniques. To simplify this non-linear phase with acceptable accuracy, we observe that the Rayleigh distance $\frac{1}{2}N^2\lambda_c$ is proportional to the square of the number of antennas, which means fewer antennas leads to a better accuracy of the far-field assumption in (4). Inspired by this observation, as illustrated in Fig. 3 (a)-(c), we propose a piecewise-far-field channel model to approximate the near-field channel. In the proposed model, the entire large array is partitioned into multiple small sub-arrays, where the number of antennas of each sub-array is much smaller than that of the entire array. With much fewer antennas, the near-field range of each sub-array significantly decreases. Therefore, even if the receiver is located in the near-field region of the entire large array, we can assume that it is in the far-field region of each sub-array.

Specifically, as shown in Fig. 3 (d), we divide the entire large array into K sub-arrays. For each sub-array, there are P adjacent antennas, so we have $N = KP$. We ignore the term (r, θ) in $\mathbf{h}(r, \theta, f_m)$ for simplicity. Then, the near-field channel is rearranged as follows

$$\mathbf{h}(f_m) = g_m [\mathbf{h}_m^{(0)}, \mathbf{h}_m^{(1)}, \dots, \mathbf{h}_m^{(K-1)}], \quad (6)$$

where $\mathbf{h}_m^{(k)} \in \mathbb{C}^{1 \times P}$ is the sub-channel between the k -th sub-array and the receiver. Denote $\delta_K^{(k)} = k - \frac{K-1}{2}$ with $k = 0, 1, \dots, K-1$, then the distance and direction between the midpoint of the k -th sub-array between the user is $r_k = \sqrt{x^2 + (y - \delta_K^{(k)}Pd)^2} = \sqrt{r^2 + (\delta_K^{(k)}Pd)^2 - 2\delta_K^{(n)}Pdr \sin \theta}$ and $\sin \theta_k = \frac{y - \delta_K^{(k)}Pd}{r_k}$, respectively. Denote $\delta_P^{(p)} = p - \frac{P-1}{2}$ with $p = 0, 1, \dots, P-1$, then according to (4), the distance $r_k^{(p)}$ between the p -th antenna in the k -th sub-array and the user can be approximated as follows

$$\begin{aligned} r_k^{(p)} &= \sqrt{x^2 + (y - (\delta_K^{(k)}P + \delta_P^{(p)})d)^2} = \sqrt{r_k^2 + (\delta_P^{(p)}d)^2 - 2\delta_P^{(p)}dr_k \sin \theta_k} \\ &\approx r_k - \delta_P^{(p)}d \sin \theta_k \end{aligned} \quad (7)$$

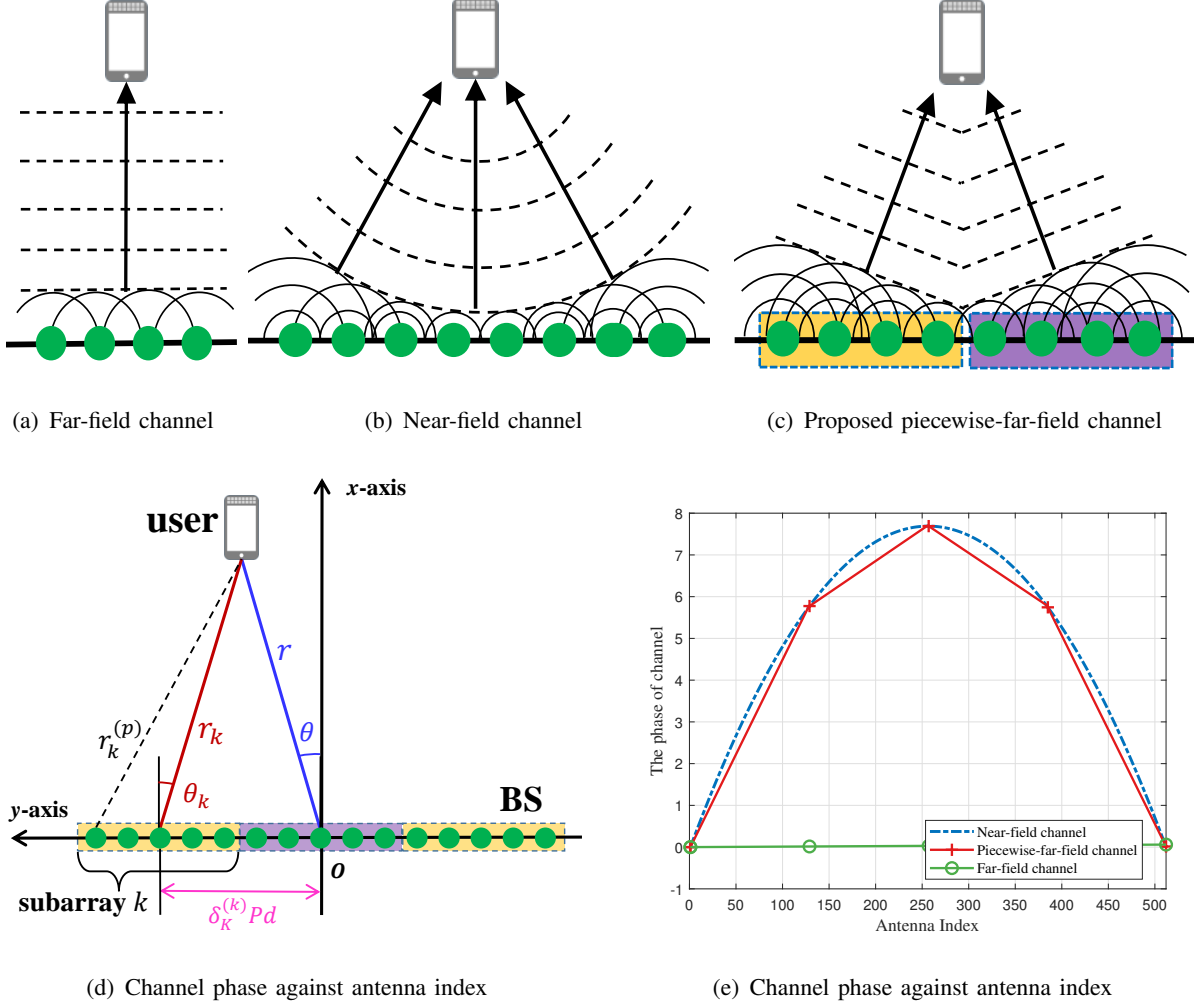


Fig. 3. Schematic diagrams of (a) far-field channel model, (b) near-field channel model, (c) piecewise-far-field channel model, and (d) channel phase against the antenna index. The number of antennas is 512, the carrier frequency is 100 GHz. The user is located at $(x, y) = (20 \text{ m}, 0 \text{ m})$. With $K = 4$ sub-arrays, the piecewise-far-field channel model can well approximate the near-field channel model.

Therefore, in the k -th sub-array, the near-field channel $\mathbf{h}_m^{(k)}$ can be approximated by a far-field channel $\tilde{\mathbf{h}}_m^{(k)}$ as below

$$[\mathbf{h}_m^{(k)}]_p = e^{-jk_m r_k} \approx e^{-jk_m r_k} e^{jk_m \delta_P^{(p)} d \sin \theta_k / c} = [\tilde{\mathbf{h}}_m^{(k)}]_p. \quad (8)$$

Denote $\eta_m = \frac{f_m}{f_c}$, since $d = \frac{\lambda_c}{2} = \frac{c}{2f_c}$ and $k_m = \frac{2\pi f_m}{c}$, we have $[\tilde{\mathbf{h}}_m^{(k)}]_p = e^{-jk_m r_k} e^{j\pi \eta_m \delta_P^{(p)} \sin \theta_k}$. In this way, the entire near-field channel can be approximated by the proposed piecewise-far-field channel model as below

$$\mathbf{h}(f_m) \approx \tilde{\mathbf{h}}(f_m) = g_m \left[\tilde{\mathbf{h}}_m^{(0)}, \tilde{\mathbf{h}}_m^{(1)}, \dots, \tilde{\mathbf{h}}_m^{(K-1)} \right]. \quad (9)$$

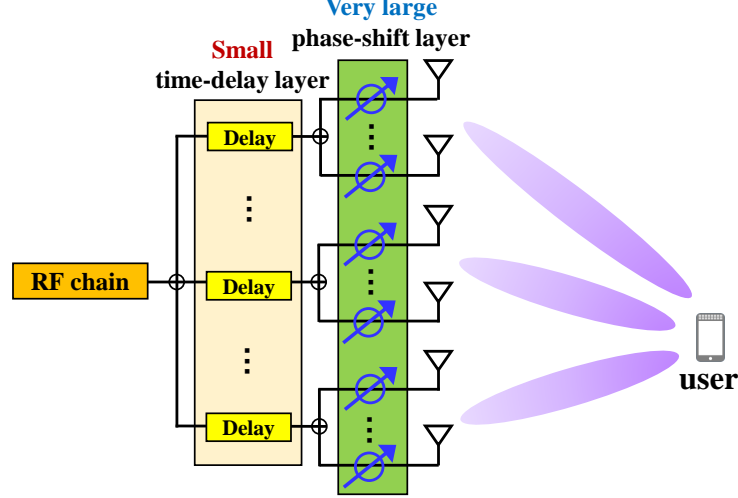


Fig. 4. Hardware architecture for the phase-delay focusing scheme to alleviate the near-field beam-split effect.

To illustrate the accuracy of the proposed model, in Fig. 3 (d), we show the channel phase as a function of the antenna index for the near-field, far-field, and piecewise-far-field channel models. The phase of the piecewise-far-field channel model can accurately approximate that of the near-field channel. The proposed channel model can be regarded as a piecewise-linearization of the existing near-field channel model, i.e., in each sub-array, the phase is linear in the antenna index. Utilizing this piecewise-linear phase characteristics, in the next subsection we will design a near-field wideband beamfocusing method referred to as phase-delay focusing to alleviate the near-field beam-split effect.

B. Proposed Phase-Delay Focusing Scheme

Based on the proposed piecewise-far-field channel model above, the approximate channel phase in (8) can be decoupled into two parts: the first part is the near-field channel phase $-k_m r_k$ across different sub-arrays, and the second part is the far-field channel phase $\pi \eta_m \delta_P^{(p)} \sin \theta_k$ within each sub-array. Both of these two parts will contribute to the near-field beam-split effect. However, since the number of antennas in a sub-array is much smaller than that in the entire array, and the performance degradation caused by beam-split is negligible when the number of antennas is small [20], [31], we can infer that the far-field channel phase $\pi \eta_m \delta_P^{(p)} \sin \theta_k$ has little effect on the near-field beam-split. Thus, our task has turned to compensating for the near-field channel phase $-k_m r_k$ to alleviate the near-field beam-split effect across different sub-arrays.

Note that the channel phase $-k_m r_k = -\frac{2\pi f_m r_k}{c}$ is linear in the frequency f_m , which can be realized by a time delay of $\frac{r_k}{c}$. Therefore, to compensate for the phase $-k_m r_k$ across different sub-arrays, as shown in Fig. 4, in each sub-array, we insert one TD element between the RF chain and the PS-based sub-array. The frequency response of a TD at f_m is $e^{-j2\pi f_m \tau'}$, where τ' is the adjustable time delay parameter. For comparison simplicity, we set $r' = c\tau'$ as the adjustable distance parameter, and then the corresponding frequency response is converted to $e^{-jk_m r'}$. Therefore, the TD is able to compensate for the frequency-dependent phase $-k_m r_k$ if $r' = -r_k$. Moreover, as shown in Fig. 4, the main function of the PS-based sub-array is to generate far-field planar waves to match the far-field phase $\pi\eta_m \delta_P^{(p)} \sin \theta_k$ within each sub-array. Through the joint control of phase and delay, the beam energy across the entire bandwidth can be approximately focused on the receiver location (r, θ) , thus we refer to this method as phase-delay focusing (PDF).

It is worth noting that the hardware architecture in Fig. 4 has also been utilized in [20] to address the far-field beam-split effect. However, since in [20] the directions θ_k and distances r_k of different sub-arrays are assumed to be identical, the beamforming method proposed in [20] can not address the near-field beam-split problem. Moreover, since the number of TD elements is much less than the number of antennas, the power consumption of the TD layer is much smaller than that of traditional massive TD arrays [31].

Specifically, since the number of TD elements is equal to the number of sub-arrays K , the wideband beamforming vector \mathbf{w}_m at frequency f_m realized by the proposed PDF method is composed of K sub-vectors, i.e.,

$$\mathbf{w}_m = \frac{1}{\sqrt{N}} \left[\mathbf{w}_m^{(0)T}, \mathbf{w}_m^{(1)T}, \dots, \mathbf{w}_m^{(K-1)T} \right]^T, \quad (10)$$

where $\mathbf{w}_m^{(k)} \in \mathbb{C}^{P \times 1}$ denotes the beamforming vector of the k -th sub-array. As shown in Fig. 4, $\mathbf{w}_m^{(k)}$ is generated by one TD unit and P PSs, which can be modeled as follows

$$\mathbf{w}_m^{(k)} = e^{-jk_m r'_k} [e^{j\pi \delta_P^{(0)} \beta'_k}, e^{j\pi \delta_P^{(1)} \beta'_k}, \dots, e^{j\pi \delta_P^{(P-1)} \beta'_k}]^T, \quad (11)$$

where r'_k denotes the adjustable distance parameter of the k -th TD unit and β'_k denotes the adjustable phase parameter of the k -th PS-based sub-array. It is clear from (11) that $\mathbf{w}_m^{(k)}$ is composed of two parts. The first part is the frequency-independent phase $\pi \delta_P^{(p)} \beta'_k$ with $p = 0, 1, \dots, P-1$ realized by the P phase shifters of the k -th sub-array, while the second part is the frequency-dependent phase $-k_m r'_k$ realized by the k th TD unit. As discussed before, $\pi \delta_P^{(p)} \beta'_k$

is designed to generate planar waves to match the far-field phase $\pi\eta_m\delta_P^{(p)}\sin\theta_k$, while the TD $t'_k = \frac{r'_k}{c}$ is designed to compensate for the near-field phase $-k_mr_k$.

Specifically, the normalized array gain achieved by the proposed PDF method can be expressed as follows

$$\begin{aligned} G_m &= \frac{1}{\sqrt{|g_m|^2 N}} |\mathbf{h}(f_m) \mathbf{w}_m| \approx \frac{1}{\sqrt{|g_m|^2 N}} |\tilde{\mathbf{h}}(f_m) \mathbf{w}_m| = \frac{1}{N} \left| \sum_{k=0}^{K-1} \tilde{\mathbf{h}}_m^{(k)} \mathbf{w}_m^{(k)} \right| \\ &= \frac{1}{N} \left| \sum_{k=0}^{K-1} e^{-jk_m(r'_k + r_k)} \sum_{p=0}^{P-1} e^{j\delta_P^{(p)}\pi(\beta'_k + \eta_m \sin\theta_k)} \right| \\ &= \frac{1}{N} \left| \sum_{k=0}^{K-1} e^{-jk_m(r'_k + r_k)} \Xi_P(\beta'_k + \eta_m \sin\theta_k) \right|, \end{aligned} \quad (12)$$

where $\Xi_P(x) = \frac{\sin(\frac{P}{2}\pi x)}{\sin(\frac{1}{2}\pi x)}$. To generate planar waves matching the sub-array channel, β_k is usually designed according to the spatial direction $\sin\theta_k$ at the center frequency [32], i.e.,

$$\beta'_k = -\eta_c \sin\theta_k = -\sin\theta_k = -\frac{y - \delta_K^k P d}{\sqrt{r^2 + (\delta_K^{(k)} P d)^2 - 2\delta_K^{(k)} P d r \sin\theta}}, \quad (13)$$

where $\eta_c = \frac{f_c}{f_c} = 1$. By substituting (13) into (12), we obtain

$$\tilde{\mathbf{h}}_m^{(k)} \mathbf{w}_m^{(k)} = e^{-k_m(r'_k + r_k)} \Xi_P((\eta_m - 1) \sin\theta_k). \quad (14)$$

The proposed PDF method aims to design r_k to maximize the array gain over the entire bandwidth to focus the beam energy on the desired location (r, θ) , thus the corresponding optimization problem can be formulated as

$$\begin{aligned} \underset{\{r_k\}}{\text{maximize}} \quad & \sum_{m=1}^M \left| \frac{1}{N} \sum_{k=0}^{K-1} e^{-jk_m(r'_k + r_k)} \Xi_P((\eta_m - 1) \sin\theta_k) \right| \\ \text{s.t.} \quad & r_k \geq 0 \quad k \in \{1, 2, \dots, K\}. \end{aligned} \quad (15)$$

We provide the following **Lemma 1** to solve optimization problem (15).

Lemma 1: If $|(\eta_m - 1) \sin\theta_k|$ at all of the sub-carrier frequencies f_m are within the main lobe of $\Xi_P(\cdot)$, i.e., $|(\eta_m - 1) \sin\theta_k| \leq |1 - \eta_m| < \frac{2}{P}, \forall m \in \{1, 2, \dots, M\}$, then the optimal solution to optimization problem (15) is

$$r'_k = L - r_k = L - \sqrt{r^2 + (\delta_K^{(k)} P d)^2 - 2\delta_K^{(k)} P d r \sin\theta}, \quad (16)$$

where L is a common distance parameter to guarantee $\min\{r'_k\} \geq 0$.

Proof: By substituting (16) into (14), the array gain of the k -th sub-array can be rewritten as

$$\tilde{\mathbf{h}}_m^{(k)} \mathbf{w}_m^{(k)} = e^{-jk_m L} \Xi_P((\eta_m - 1) \sin \theta_k). \quad (17)$$

Since $|(\eta_m - 1) \sin \theta_k| \leq |\eta_m - 1| < \frac{2}{P}$, then it is obvious that $\Xi_P((\eta_m - 1) \sin \theta_k) > 0$. In this case, the array gain can be rewritten as

$$\left| \sum_k \tilde{\mathbf{h}}_m^{(k)} \mathbf{w}_m^{(k)} \right| = \sum_k \Xi_P((\eta_m - 1) \sin \theta_k). \quad (18)$$

In addition, based on the Cauchy-Schwarz inequality, we can derive the upper bound on the array gain as follows

$$\left| \sum_k \tilde{\mathbf{h}}_m^{(k)} \mathbf{w}_m^{(k)} \right| \leq \sum_k \left| \tilde{\mathbf{h}}_m^{(k)} \mathbf{w}_m^{(k)} \right| = \sum_k \Xi_P((\eta_m - 1) \sin \theta_k). \quad (19)$$

It is clear from (18) and (19) that r'_k is the optimal solution to $\left| \sum_k \tilde{\mathbf{h}}_m^{(k)} \mathbf{w}_m^{(k)} \right|$ at frequency f_m . Moreover, since r'_k is frequency independent, it is the optimal solution to all sub-carriers. Therefore, r'_k is the optimal solution to problem (15), which completes the proof. ■

To sum up, (13) and (16) complete the design of the proposed PDF scheme. In **Lemma 1**, we assume $|(\eta_m - 1) \sin \theta_k| \leq |\eta_m - 1| < \frac{2}{P}$, thus, the number of antennas of a sub-array P can not be very large. In the next section, we will further discuss how to design the parameter P in detail.

IV. THEORETICAL ANALYSIS

In this section, we first theoretically analyze the achievable array gain of the proposed PDF method. Then, a more accurate effective Rayleigh distance for distinguishing the far-field and near-field region is defined from the perspective of array gain. Finally, based on the above two conclusions, we discuss how to design the number of antennas of each sub-array.

A. Array Gain performance

To better understand whether the proposed PDF method can mitigate the near-field beam split effect, we will derive the normalized array gain achieved by the proposed PDF method over the entire bandwidth. By adopting the solutions of β'_k and t'_k in (13) and (16), the approximate normalized array gain can be obtained in the following **proposition 1**.

Proposition 1: Suppose $|(\eta_m - 1) \sin \theta_k|$ at all of the sub-carrier frequencies f_m are within the main lobe of $\Xi_P(\cdot)$, i.e., $|(\eta_m - 1) \sin \theta_k| \leq |1 - \eta_m| < \frac{2}{P}, \forall m \in \{1, 2, \dots, M\}$. Then, if a

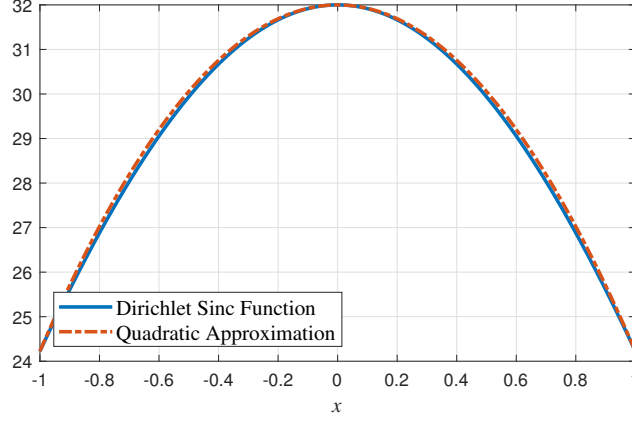


Fig. 5. Quadratic approximation $P - (P - \Xi_P(1 - \eta_m))x^2$ of the Dirichlet sinc function $\Xi_P((1 - \eta_M)x)$, where $x \in [-1, 1]$ and $P = 32$.

user is located in the far-field region of a sub-array, the normalized array gain achieved by the proposed PDF method can be approximated as

$$G_m = \frac{1}{\sqrt{|g_m|^2 N}} |\mathbf{h}(f_m) \mathbf{w}_m| \approx \left(1 - \frac{\sum_{k=0}^{K-1} \cos^2 \theta_k}{K}\right) \frac{\Xi_P(1 - \eta_m)}{P} + \frac{\sum_{k=0}^{K-1} \cos^2 \theta_k}{K}. \quad (20)$$

Proof: Referring to (18), the array gain G_m achieved by the proposed PDF method can be approximated as

$$G_m = \frac{1}{\sqrt{|g_m|^2 N}} |\mathbf{h}(f_m) \mathbf{w}_m| \approx \frac{1}{\sqrt{|g_m|^2 N}} |\tilde{\mathbf{h}}(f_m) \mathbf{w}_m| = \frac{1}{N} \sum_{k=0}^{K-1} \Xi_P((\eta_m - 1) \sin \theta_k). \quad (21)$$

It is difficult to calculate the sum of the Dirichlet function. As shown in Fig. 5, we utilize a polynomial to fit function $\Xi_P((\eta_m - 1)x)$ by three points $(-1, \Xi_P(\eta_m - 1))$, $(0, P)$, and $(1, \Xi_P(\eta_m - 1))$, then we have

$$\Xi_P((\eta_m - 1)x) \approx P - (P - \Xi_P(\eta_m - 1))x^2. \quad (22)$$

In this way, the normalized array gain can be rewritten as follows

$$\begin{aligned} G_m &\approx 1 - \frac{P - \Xi_P(\eta_m - 1)}{N} \sum_{k=0}^{K-1} \sin^2 \theta_k = 1 - \frac{P - \Xi_P(\eta_m - 1)}{N} \sum_{k=0}^{K-1} (1 - \cos^2 \theta_k) \\ &= \left(1 - \frac{\sum_{k=0}^{K-1} \cos^2 \theta_k}{K}\right) \frac{\Xi_P(1 - \eta_m)}{P} + \frac{\sum_{k=0}^{K-1} \cos^2 \theta_k}{K}. \end{aligned} \quad (23)$$

Therefore, the approximation (20) in **Proposition 1** is proved. ■

It can be observed from (20) that

$$\frac{\sum_{k=0}^{K-1} \cos^2 \theta_k}{K} \geq \min_k \{\cos^2 \theta_k\}. \quad (24)$$

By combining (20) and (24), since $\frac{\Xi_P(1-\eta_m)}{P} < 1$, we obtain the following lower bound for the normalized array gain

$$G_m \geq G_m^{\text{LB}} = \left(1 - \min_k \{\cos^2 \theta_k\}\right) \frac{\Xi_P(1 - \eta_m)}{P} + \min_k \{\cos^2 \theta_k\}. \quad (25)$$

The lower bound in (25) solely depends on the number of sub-array antennas P , rather than the entire number of antennas N . This observation confirms that by inserting one TD into each sub-array, the near-field beam split among different sub-arrays is effectively eliminated. Meanwhile, the sole array gain loss term $\Xi_P(1 - \eta_m)/P$ is caused by the near-field beam split within each sub-array. Since P is smaller than the entire number of antennas N , the near-field beam split within each sub-array is slight and acceptable. For instance, if the bandwidth B is 5 GHz, the carrier frequency f_c is 100 GHz, then the maximum $|\eta_m - 1|$ is $\frac{B}{2f_c} = 0.025$. For a 512-antenna array, if we divide this array into $K = 16$ sub-arrays, then the number of sub-array antennas is $P = 32$. By assuming that the typical sector range of a BS is $[-\frac{\pi}{3}, \frac{\pi}{3}]$, we obtain $\min_{\theta_k} \{\cos^2 \theta_k\} = \cos^2 \frac{\pi}{3} = \frac{1}{4}$. Based on the parameters above, the lower bound g_m^{LB} is larger than 0.82 according to (25), which means the array gain loss is less than 18% across the entire wideband. Thus we can conclude that the near-field beam split effect can be effectively alleviated.

B. Definition of the Effective Rayleigh distance

In the previous sub-section, we assume the user is located in the near-field range of the entire array, but in the far-field range of each sub-array. Therefore, it is essential to identify the near-field ranges of a sub-array and the entire array. As mentioned before, it is a standard way to utilize the classical Rayleigh distance to calculate the near-field range. However, in our simulations, we observe that the Rayleigh distance overestimates the actual near-field range. For example, when the array aperture is $D = 0.76$ meters, and the carrier is $f_c = 100$ GHz, the Rayleigh distance is around 400 meters, but the far-field wideband beamforming method [20] will not suffer from an obvious rate loss until the distance is less than 120 meters. This observation implies that, the classical Rayleigh distance is not accurate in distinguishing near-field and far-field when evaluating transmission rate. This is because the classical Rayleigh distance is derived from the view of maximum phase error, which does not directly influence the transmission rate. In contrast, since the near-field effect directly impacts array gain, and array gain directly determines

the transmission rate, a more accurate metric to define the near-field range from the perspective of array gain is needed.

Specifically, we first introduce the derivation of the classical Rayleigh distance from the view of phase error. Without loss of generality, we only considers the center frequency f_c . The near-field channel on the n -th antenna is $[\mathbf{h}(r, \theta, f_c)]_n = g_c e^{-k_c r^{(n)}} = g_c e^{-k_c(r^2 + (\delta_N^{(n)} d)^2 - 2\delta_N^{(n)} d r \sin \theta)^{0.5}}$, where g_c denotes the path loss at the center frequency. By utilizing the far-field approximation in (4), the far-field channel is derived as $[\mathbf{h}_{\text{far}}(r, \theta, f_c)]_n = [\mathbf{h}(+\infty, \theta, f_c)]_n = g_c e^{-jk_c(r - \delta_N^{(n)} d \sin \theta)}$. Therefore, the phase error between $[\mathbf{h}(r, \theta, f_c)]_n$ and $[\mathbf{h}_{\text{far}}(r, \theta, f_c)]_n$ is defined as $E_n(r, \theta) = |\angle[\mathbf{h}(r, \theta, f_c)]_n - \angle[\mathbf{h}_{\text{far}}(r, \theta, f_c)]_n| = |k_c r^{(n)} - k_c(r - \delta_N^{(n)} d \sin \theta)|$. Then, the Rayleigh distance is defined as follows [17]: if the distance r between the user and the BS is larger than the Rayleigh distance R , then the maximum phase error $E(r) = \max_{n, \theta} E_n(r, \theta)$ is no more than $\frac{\pi}{8}$. That is to say, if the maximum phase error $E(r)$ is larger than $\frac{\pi}{8}$, then the user is in the near-field region of the BS. To derive the close form of $E(r)$, the second order Taylor expansion $(1+x)^{\frac{1}{2}} \approx 1 + \frac{1}{2}x - \frac{1}{8}x^2$ is widely considered [17]. By this means, the distance $r^{(n)}$ can be approximated as

$$r^{(n)} \approx \sqrt{r^2 - 2r\delta_N^{(n)} d \sin \theta + (\delta_N^{(n)} d)^2} \stackrel{(a)}{\approx} r - \delta_N^{(n)} d \sin \theta + \frac{(\delta_N^{(n)} d)^2 \cos^2 \theta}{2r}. \quad (26)$$

Then the phase error is approximated as $E_n(r, \theta) \approx k_c \frac{(\delta_N^{(n)} d)^2 \cos^2 \theta}{2r}$. Since $\delta_N^{(n)} = n - \frac{N-1}{2}$ with $n = 0, 1, \dots, N-1$, and $\cos^2 \theta \leq 1$, we have $E(r) = \max_{n, \theta} E_n(r, \theta) = k_c \frac{(0.5(N-1)d)^2}{2r}$. As the array aperture is $D = (N-1)d$ and $k_c = \frac{2\pi f_c}{c} = \frac{2\pi}{\lambda_c}$, we have $E(r) = \frac{D^2 \pi}{4r \lambda_c}$. Obviously, when the distance $r > R = \frac{2D^2}{\lambda_c}$, the maximum phase error is no more than $\frac{\pi}{8}$. Therefore, the Rayleigh distance is $R = \frac{2D^2}{\lambda_c}$.

On the other hand, we define a new effective Rayleigh distance from the perspective of array gain. Specifically, the normalized coherence between the channel $\mathbf{h}(r, \theta, f_c) \in \mathbb{C}^{1 \times N}$ and its far-field approximation $\mathbf{h}_{\text{far}}(r, \theta, f_c) \in \mathbb{C}^{1 \times N}$ is evaluated as $\mu(r, \theta) = \frac{1}{g_c^2 N} |\mathbf{h}(r, \theta, f_c) \mathbf{h}_{\text{far}}(r, \theta, f_c)^H|$. The coherence $\mu(r, \theta)$ equivalents to the achievable array gain if the BS utilizes the far-field beamforming vector $\mathbf{w} = \frac{1}{g_c \sqrt{N}} \mathbf{h}_{\text{far}}(r, \theta, f_c)^H$ with planar wavefront to serve a user located at (r, θ) . Then, the effective Rayleigh distance is defined as follows: if the distance r between the user and the BS is larger than the effective Rayleigh distance R_{eff} , then the corresponding coherence $\mu(r, \theta)$ is not less than 95% (note that this threshold can be changed). Since the array gain $\mu(r, \theta)$ directly influence the transmission rates, R_{eff} can be a more accurate near-field range in communication systems.

To obtain the value of the effective Rayleigh distance, we need to derive the close form of $\mu(r, \theta)$. Based on the second order Taylor expansion in (26), $\mu(r, \theta)$ can be expressed as

$$\begin{aligned}\mu(r, \theta) &= \frac{1}{N} \left| \sum_{n=0}^{N-1} e^{-jk_c(r^{(n)} - (r - \delta_N^{(n)} d \sin \theta))} \right| \approx \frac{1}{N} \left| \sum_{n=0}^{N-1} e^{-j\pi \frac{(\delta_N^{(n)} d)^2 \cos^2 \theta}{\lambda_c r}} \right| \\ &= \frac{1}{N} \left| \sum_{n=0}^{N-1} e^{-j\pi \frac{(n - \frac{N-1}{2})^2 d^2 \cos^2 \theta}{\lambda_c r}} \right| = \frac{1}{N} \left| \sum_{n=-\frac{N-1}{2}}^{\frac{N-1}{2}} e^{-j\pi \frac{(nd)^2 \cos^2 \theta}{\lambda_c r}} \right| \\ &= \frac{1}{N} \left| \sum_{m=-\frac{1}{2} + \frac{1}{2N}}^{\frac{1}{2} - \frac{1}{2N}} e^{-j\pi \frac{m^2 (Nd)^2 \cos^2 \theta}{\lambda_c r}} \right|. \quad (27)\end{aligned}$$

Notice that the operator $\sum_{m=-\frac{1}{2} + \frac{1}{2N}}^{\frac{1}{2} - \frac{1}{2N}}$ calculates the summation with $m = -\frac{1}{2} + \frac{1}{2N}, -\frac{1}{2} + \frac{3}{2N}, -\frac{1}{2} + \frac{5}{2N}, \dots, \frac{1}{2} - \frac{1}{2N}$. Denote $x = \frac{N^2 d^2 \cos^2 \theta}{\lambda_c r}$ and $\Delta_m = \frac{1}{N}$, since the number of antennas N is very large, (27) can be represented as

$$\mu(r, \theta) = \left| \sum_{m=-\frac{1}{2} + \frac{1}{2N}}^{\frac{1}{2} - \frac{1}{2N}} e^{-j\pi m^2 x \Delta_m} \right| \stackrel{N \rightarrow +\infty}{=} \left| \int_{-1/2}^{1/2} e^{-j\pi m^2 x} dm \right| = 2 \left| \int_0^{1/2} e^{-j\pi m^2 x} dm \right|. \quad (28)$$

Finally, denote $\frac{1}{2}t^2 = m^2 x$, then $\mu(r, \theta)$ can be rewritten as

$$\mu(r, \theta) = \frac{2}{\sqrt{2x}} \left| \int_0^{\frac{\sqrt{2x}}{2}} e^{-j\frac{1}{2}\pi t^2} dt \right| = G(\beta), \quad (29)$$

where $G(\beta) = \left| \int_0^\beta e^{-j\frac{1}{2}\pi t^2} dt \right| / \beta$ and $\beta = \frac{\sqrt{2x}}{2} = \sqrt{\frac{N^2 d^2 \cos^2 \theta}{2\lambda_c r}}$. It is clear from (29) that the coherence heavily relies on the characteristics of the function $G(\beta)$. Fortunately, $G(\beta)$ does not contain any parameters, thus it is sufficient to obtain its numerical result by offline integration.

As shown in Fig. 6, the function $G(\beta)$ shows a significant downward trend. If we desire the coherence $\mu(r, \theta) = G(\beta) > 0.95$, we approximately obtain $\beta < \beta_\Delta$ where $\beta_\Delta = 0.8257$ is derived by solving $|G(\beta_\Delta)| = 0.95$. Moreover, since the array aperture is $D = (N - 1)d \approx Nd$ and $\beta = \sqrt{\frac{N^2 d^2 \cos^2 \theta}{2\lambda_c r}}$, we have $r \geq \frac{N^2 d^2 \cos^2 \theta}{2\beta_\Delta^2 \lambda} = 0.367 \cos^2 \theta \frac{2D^2}{\lambda_c}$. That is to say, on any direction θ , if the distance r is larger than $0.367 \cos^2 \theta \frac{2D^2}{\lambda_c}$, then the corresponding array gain $\mu(r, \theta)$ achieved by the far-field beam is larger than 0.95. Therefore, the effective Rayleigh distance is

$$R_{\text{eff}} = \epsilon \cos^2 \theta \frac{2D^2}{\lambda}, \quad (30)$$

where $\epsilon = 0.367$. It is obvious from (30) that, the effective Rayleigh distance is less than the Rayleigh distance, and it is also related to the direction θ . Since the effective Rayleigh distance is defined from the perspective of array gain that directly affects the transmission rate, it is a

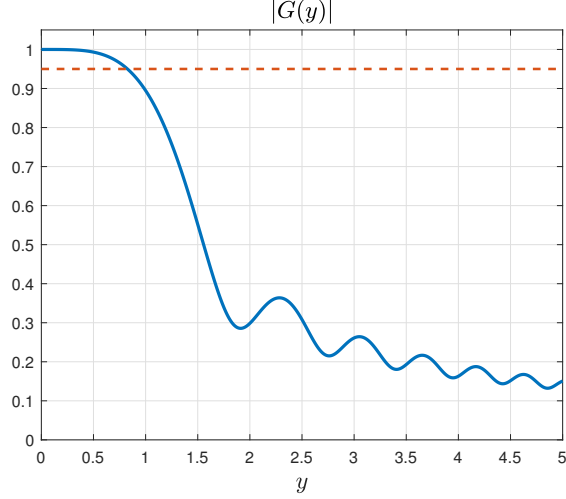


Fig. 6. The numerical results of $G(\beta)$

more accurate metric to determine the near-field range for practical communications. In Section V, the accuracy of the effective Rayleigh distance will be verified, e.g., the existing far-field beamforming scheme [20] will actually suffer from an obvious rate loss when the distance is exactly less than the effective Rayleigh distance.

C. Design the Number of Antennas of a Sub-array

In this part, we focus on designing the number of antennas of each sub-array P , which is the most important design parameter of the proposed PDF method. Firstly, to satisfy the assumptions in **Lemma 1**, all of the direction deviations should be smaller than $\frac{2}{P}$, so we have $\max |\eta_m - 1| = |\eta_M - 1| = \frac{B}{2f_c} \leq \frac{2}{P}$. Then, according to **Proposition 1**, the receiver should be located in the far-field region of each sub-array. The array aperture of each sub-array is $\frac{D}{P}$. Define ρ_{\min} as the minimum allowable distance between the receiver and the BS, then according to the effective Rayleigh distance provided in (30), we have $\rho_{\min} \geq \max_{\theta} R_{\text{eff}} = 0.367 \frac{2(D/P)^2}{\lambda_c} \approx 0.183 P^2 \lambda_c$. Finally, based on the lower bound derived in (25), if the minimum allowable array gain is γ , then $G_m^{\text{LB}} \geq \gamma$ should be satisfied.

In conclusion, according to the three requirements above, the number of antennas of each sub-array P should satisfy

$$P \leq \min \left\{ \frac{4f_c}{B}, \sqrt{\frac{\rho}{0.183\lambda_c}}, P_{\gamma} \right\}, \quad (31)$$

where P_{γ} is obtained by solving the transcendental equation $G_m^{\text{LB}} = \gamma$ in (25). For instance, if the bandwidth and carrier are $B = 5$ GHz and $f_c = 100$ GHz. The minimum distance ρ_{\min} is 1

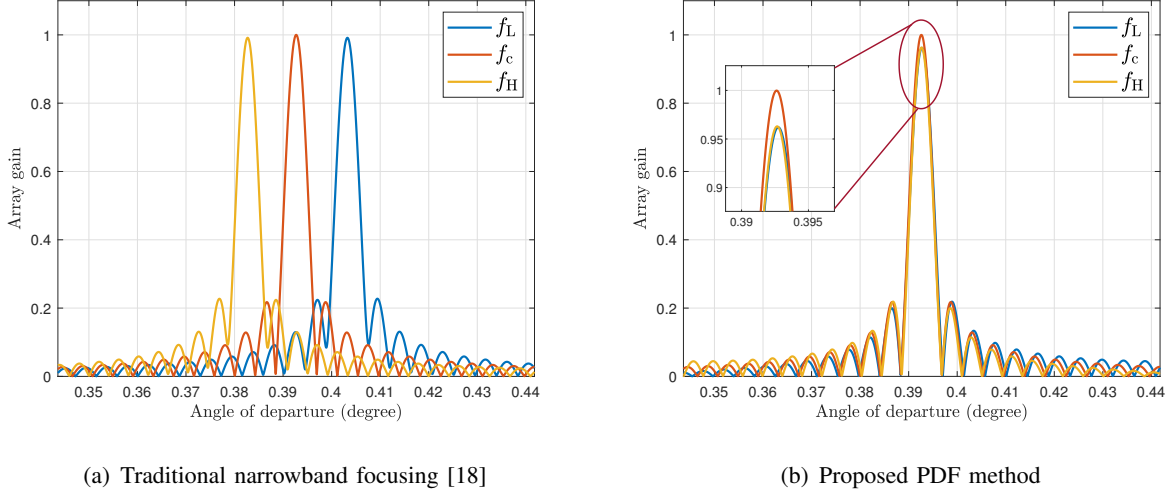


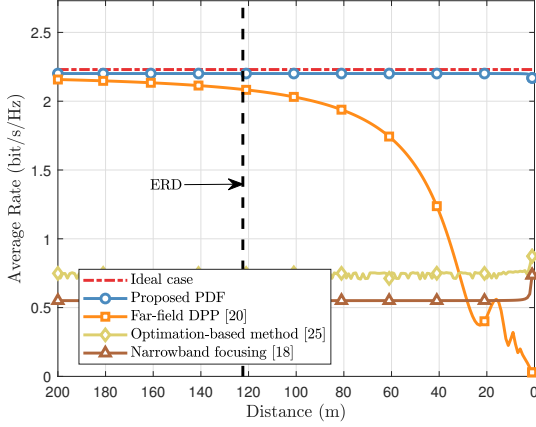
Fig. 7. Array gain performance against AoD with fixed distance.

meter and the minimum allowable array gain γ is 80%, then we have $\frac{4f_c}{B} = 80$, $\sqrt{\frac{\rho}{0.183\lambda_c}} \approx 43$ and $P_\gamma \approx 33$. Therefore, for the above typical system settings, the number of antennas of a sub-array is $P = 32$. This means if a 512-antenna array is deployed, then only $K = \frac{512}{32} = 16$ TDs are enough to alleviate the near-field beam split effect.

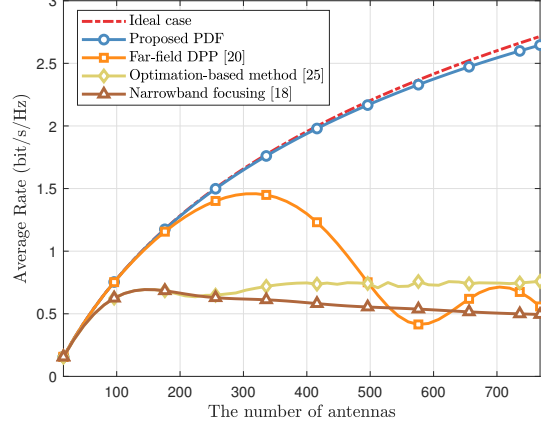
V. SIMULATION RESULTS

In this section, simulation results are provided to verify the performance of the proposed PDF method. The center frequency and bandwidth are $f_c = 100$ GHz and $B = 5$ GHz, respectively. The number of sub-carriers is $M = 256$. Without special statements, the number of antennas is $N = 512$, which can be implemented by radio stripes. As analyzed in Section IV, the number of sub-arrays is $K = 16$.

Fig. 7 shows the array gain performance for different sub-carriers as a function of the angle of departure (AoD) for a fixed distance. Fig. 7 (a) considers the traditional near-field narrowband focusing method [18], while Fig. 7(b) considers the proposed PDF method. We use f_L , f_c , and f_H to denote the lowest, the center, and the highest frequency, respectively. The beam energy is supposed to be focused on location $(r, \theta) = (10 \text{ m}, \frac{\pi}{8})$. For the traditional narrowband focusing scheme [18], the near-field beam-split effect causes the beams at f_L , f_c , and f_H to be focused on different locations. However, the proposed PDF method can effectively focus the energy of



(a) Average rate versus distance



(b) Average rate versus the number of BS antenna

Fig. 8. Average rate performance comparison. In (a), the number of antennas is $N = 512$. The receiver is moved from $(r_1, \theta) = (200 \text{ m}, \frac{\pi}{8})$ to $(r_2, \theta) = (0.5 \text{ m}, \frac{\pi}{8})$ in a straight line. In (b), the receiver is located at $(r, \theta) = (30 \text{ m}, \frac{\pi}{8})$. The number of sub-arrays is fixed to $K = 16$, and the number of antennas is gradually increasing from 16 to 1024.

the beams at f_L , f_c , and f_H at the desired receiver location, and the beams at f_L and f_H achieve more than 95% of the maximum array gain at the desired location.

We further evaluate the average rate performance $C = \frac{1}{M} \sum_{m=1}^M \log_2 \left(1 + \frac{P_T}{\sigma^2} |\mathbf{h}(f_m) \mathbf{w}_m|^2 \right)$, where the transmit signal-to-noise ratio $\text{SNR} = \frac{P_T}{\sigma^2}$ is 25 dB. In Fig. 8, we compare the average rate achieved by the proposed PDF method with that achieved by existing schemes, including the ideal case realized by a massive TD array, narrowband focusing [18], an optimization-based method [25], and the far-field beam-split solution delay-phase-precoding (DPP) [20]. The average rate versus the distance r is shown in Fig. 8 (a). To explicitly illustrate the impact of the near-field effect, we ignore the large-scale path loss so that the average rate achieved by the massive TD array does not change with the distance. The receiver is moved from $(200 \text{ m}, \frac{\pi}{8})$ to $(0.5 \text{ m}, \frac{\pi}{8})$. The average rate of the proposed PDF scheme approaches the ideal case with a rate loss of less than 1%. It is worth noting that with 512 antenna elements at frequency $f_c = 100 \text{ GHz}$, the classical Rayleigh distance is around 300 meters. However, in Fig. 8 (a), the far-field method DPP [20] will not suffer from an obvious rate loss until the distance is less than 120 meters, which implies when evaluating the achievable rate, the Rayleigh distance is not accurate to distinguish the far-field and near-field regions. This is because the Rayleigh distance is derived based on the phase error [17], which does not directly affect the achievable rate. By contrast, since the array gain directly affect the achievable rate, the newly defined effective Rayleigh distance (30) is a

more accurate metric to identify the near-field range for practical communications. As shown in Fig. 8 (a), the average rate of the far-field method DPP [20] actually becomes degraded when the distance is less than the effective Rayleigh distance.

Finally, the average rate versus the number of BS antennas is shown in Fig. 8 (b). The receiver is located at $(r, \theta) = (30 \text{ m}, \frac{\pi}{8})$. The number of antennas is gradually increasing from 16 to 1024. As the BS array aperture increases, all existing schemes suffer from a severe rate loss compared to the ideal case. However, the proposed PDF scheme achieves near-optimal performance in the entire range of the number of antennas. Therefore, the near-field beam-split effect is effectively alleviated.

VI. CONCLUSIONS

In this paper, we reveal an important challenge for future communication systems employing extremely large array, i.e., near-field beam-split. To address this challenge, we first propose a piecewise-far-field model to approximate the near-field channel with high accuracy. Based on this model, we propose a PDF method through joint phase and delay control to significantly alleviate the near-field beam-split effect. Moreover, we further define a new effective Rayleigh distance from the perspective of the array gain, which is more accurate for distinguishing the near-field range than the classical Rayleigh distance for practical communications. Finally, numerical results are provided to demonstrate the effectiveness of our work. For future works, we may consider the near-field wideband channel estimation [33] and dynamic beam tracking under mobility [30].

REFERENCES

- [1] R. W. Heath, N. González-Prelcic, S. Rangan, W. Roh, and A. M. Sayeed, "An overview of signal processing techniques for millimeter wave MIMO systems," *IEEE J. Sel. Topics Signal Process.*, vol. 10, no. 3, pp. 436–453, Apr. 2016.
- [2] E. D. Carvalho, A. Ali, A. Amiri, M. Angjelichinoski, and R. W. Heath, "Non-stationarities in extra-large-scale massive MIMO," *IEEE Wireless Commun.*, vol. 27, no. 4, pp. 74–80, Aug. 2020.
- [3] "Radio stripes: re-thinking mobile networks," 2019. [Online]. Available: <https://www.ericsson.com/en/blog/2019/2/radio-stripes>.
- [4] W. Tang, M. Z. Chen, X. Chen, J. Y. Dai, Y. Han, M. Di Renzo, Y. Zeng, S. Jin, Q. Cheng, and T. J. Cui, "Wireless communications with reconfigurable intelligent surface: Path loss modeling and experimental measurement," *IEEE Trans. Wireless Commun.*, vol. 20, no. 1, pp. 421–439, Jan. 2021.
- [5] L. Zhang, M. Z. Chen, W. Tang, J. Y. Dai, L. Miao, X. Y. Zhou, S. Jin, Q. Cheng, and T. J. Cui, "A wireless communication scheme based on space- and frequency-division multiplexing using digital metasurfaces," *Nat. Electron.*, vol. 4, p. 218–227, Mar. 2021.

- [6] S. Nie, J. M. Jornet, and I. F. Akyildiz, "Intelligent environments based on ultra-massive MIMO platforms for wireless communication in millimeter wave and terahertz bands," in *Proc. IEEE International Conference on Acoustics, Speech and Signal Processing (IEEE ICASSP'19)*, May 2019, pp. 7849–7853.
- [7] A. R. Ndjiongue, T. M. N. Ngatched, O. A. Dobre, and H. Haas, "Towards the use of reconfigurable intelligent surfaces in VLC systems: Beam steering," *arXiv preprint arXiv:2009.06822*, Sep. 2020.
- [8] V. Arun and H. Balakrishnan, "Rfocus: Beamforming using thousands of passive antennas," in *Proc. 17th USENIX Symposium on Networked Systems Design and Implementation (NSDI'20)*, Feb. 2020, pp. 1047–1061.
- [9] A. Liao, Z. Gao, Y. Yang, H. H. Nguyen, H. Wang, and H. Yin, "Angle estimation for terahertz ultra-massive MIMO-based space-to-air communications," *arXiv preprint arXiv:2108.00675*, Aug. 2021.
- [10] S. J. Maeng, Y. Yapiıcı, İsmail Güvenç, A. Bhuyan, and H. Dai, "Precoder design for physical-layer security and authentication in massive MIMO UAV communications," *arXiv preprint arXiv:2107.00799*, Jul. 2021.
- [11] S. Koenig, D. Lopez-Diaz, J. Antes, F. Boes, R. Henneberger, A. Leuther, A. Tessmann, R. Schmogrow, D. Hillerkuss, R. Palmer, T. Zwick, C. Koos, W. Freude, O. Ambacher, J. Leuthold, and I. Kallfass, "Wireless sub-THz communication system with high data rate," *Nat. Photonics*, vol. 7, p. 977–981, Oct. 2013.
- [12] H. Elayan, O. Amin, B. Shihada, R. M. Shubair, and M. Alouini, "Terahertz band: The last piece of RF spectrum puzzle for communication systems," *IEEE Open J. Commun. Society*, vol. 1, pp. 1–32, 2020.
- [13] T. S. Rappaport, Y. Xing, O. Kanhere, S. Ju, A. Madanayake, S. Mandal, A. Alkhateeb, and G. C. Trichopoulos, "Wireless communications and applications above 100 GHz: Opportunities and challenges for 6G and beyond," *IEEE Access*, vol. 7, pp. 78 729–78 757, 2019.
- [14] Z. Zhou, X. Gao, J. Fang, and Z. Chen, "Spherical wave channel and analysis for large linear array in LoS conditions," in *Proc. IEEE Globecom Workshops 2015*, Dec. 2015, pp. 1–6.
- [15] B. Friedlander, "Localization of signals in the near-field of an antenna array," *IEEE Trans. Signal Process.*, vol. 67, no. 15, pp. 3885–3893, Aug. 2019.
- [16] D. Tse and P. Viswanath, *Fundamentals of Wireless Communication*. Cambridge, U.K.: Cambridge Univ. Press, 2005.
- [17] K. T. Selvan and R. Janaswamy, "Fraunhofer and fresnel distances: Unified derivation for aperture antennas," *IEEE Antennas Propag. Mag.*, vol. 59, no. 4, pp. 12–15, Aug. 2017.
- [18] D. Headland, Y. Monnai, D. Abbott, C. Fumeaux, and W. Withayachumnankul, "Tutorial: Terahertz beamforming, from concepts to realizations," *APL Photonics*, vol. 3, p. 051101, May 2018.
- [19] F. Sohrabi and W. Yu, "Hybrid analog and digital beamforming for mmWave OFDM large-scale antenna arrays," *IEEE J. Sel. Areas Commun.*, vol. 35, no. 7, pp. 1432–1443, Jul. 2017.
- [20] L. Dai, J. Tan, and H. V. Poor, "Delay-phase precoding for wideband THz massive MIMO," *arXiv preprint arXiv:2102.05211*, Feb. 2021.
- [21] X. Gao, L. Dai, S. Zhou, A. M. Sayeed, and L. Hanzo, "Wideband beamspace channel estimation for millimeter-wave MIMO systems relying on lens antenna arrays," *IEEE Trans. Signal Process.*, vol. 67, no. 18, pp. 4809–4824, Jul. 2019.
- [22] G. Yasaman, S. Rabi, C. Aaron, K. Edward, and M. Daniel, "Single-shot link discovery for terahertz wireless networks," *Nat. Commun.*, vol. 11, no. 1, pp. 1–6, Apr. 2020.
- [23] Y. Chen, Y. Xiong, D. Chen, T. Jiang, S. X. Ng, and L. Hanzo, "Hybrid precoding for wideband millimeter wave MIMO systems in the face of beam squint," *IEEE Trans. Wireless Commun.*, vol. 20, no. 3, pp. 1847–1860, Mar. 2021.
- [24] X. Liu and D. Qiao, "Space-time block coding-based beamforming for beam squint compensation," *IEEE Wireless Commun. Lett.*, vol. 8, no. 1, pp. 241–244, Feb. 2019.
- [25] X. Yu, J. Shen, J. Zhang, and K. B. Letaief, "Alternating minimization algorithms for hybrid precoding in millimeter wave MIMO systems," *IEEE J. Sel. Topics Signal Process.*, vol. 10, no. 3, pp. 485–500, Mar. 2016.

- [26] H. Hashemi, T. Chu, and J. Roderick, "Integrated true-time-delay-based ultra-wideband array processing," *IEEE Commun. Mag.*, vol. 46, no. 9, pp. 162–172, Sep. 2008.
- [27] C. Lin, G. Y. Li, and L. Wang, "Subarray-based coordinated beamforming training for mmWave and sub-THz communications," *IEEE J. Sel. Areas Commun.*, vol. 35, no. 9, pp. 2115–2126, Sep. 2017.
- [28] J. Sherman, "Properties of focused apertures in the Fresnel region," *IRE Trans. Antennas Propag.*, vol. 10, no. 4, pp. 399–408, Jul. 1962.
- [29] D. Fattal, J. Li, Z. Peng, M. Fiorentino, and R. G. Beausoleil, "Flat dielectric grating reflectors with focusing abilities," *Nat. Photonics*, vol. 4, p. 466–470, May 2010.
- [30] J. Tan and L. Dai, "Wideband beam tracking in THz massive MIMO systems," *IEEE J. Sel. Areas Commun.*, vol. 39, no. 6, pp. 1693–1710, Jun. 2021.
- [31] R. J. Mailloux, *Phased Array Antenna Handbook*. Norwood, MA, USA: Artech House, 2005.
- [32] S. Mumtaz, J. Rodriguez, and L. Dai, *MmWave Massive MIMO: A Paradigm for 5G*. Academic Press, Elsevier, 2016.
- [33] M. Cui and L. Dai, "Channel estimation for extremely large-scale MIMO: Far-Field or Near-Field?" *arXiv preprint arXiv:2108.07581*, Aug. 2021.